Small Molecule-Mediated Control of Hydroxyapatite Growth: Free Energy Calculations Benchmarked to Density Functional Theory

Zhijun Xu,*[a] Yang Yang,[b] Ziqiu Wang,[a] Donald Mkhonto,[c] Cheng Shang,[d] Zhi-Pan Liu,[d] Qiang Cui,[e] and Nita Sahai*[a]

The unique, plate-like morphology of hydroxyapatite (HAP) nanocrystals in bone lends to the hierarchical structure and functions of bone. Proteins enriched in phosphoserine (Ser-OPO_3) and glutamic acid (Glu) residues have been proposed to regulate crystal morphology; however, the atomic-level mechanisms remain unclear. Previous molecular dynamics studies addressing biomineralization have used force fields with limited benchmarking, especially at the water/mineral interface, and often limited sampling for the binding free energy profile. Here, we use the umbrella sampling/weighted histogram analysis method to obtain the adsorption free energy of Ser-OPO_3 and Glu on HAP (100) and (001) surfaces to understand organic-mediated crystal growth. The calculated organic-water–mineral interfacial energies are carefully benchmarked to density functional theory calculations, with explicit inclusion of solvating water molecules around the adsorbate plus the Poisson–Boltzmann continuum model for long-range solvation effects. Both amino acids adsorb more strongly on the HAP (100) face than the (001) face. Growth rate along the [100] direction should then be slower than in the [001] direction, resulting in plate-like crystal morphology with greater surface area for the (100) than the (001) face, consistent with bone HAP crystal morphology. Thus, even small molecules are capable of regulating bone crystal growth by preferential adsorption in specific directions. Furthermore, Ser-OPO_3 is a more effective growth modifier by adsorbing more strongly than Glu on the (100) face, providing one possible explanation for the energetically expensive process of phosphorylation of some proteins involved in bone biomineralization. The current results have broader implications for designing routes for biomimetic crystal synthesis. © 2013 Wiley Periodicals, Inc.

DOI: 10.1002/jcc.23474

Introduction

Hydroxyapatite (HAP, $Ca_{10}(PO_4)_6(OH)_2$) is the idealized stoichiometry for the main mineral component of bone and tooth enamel, and the HAP crystals are in specific structural registry with the main protein component, collagen.[1] The crystals in these two mineralized tissues have different microstructural morphologies, varying degrees of nonideal stoichiometry, different spatial relationship with collagen, and different arrangement of the collagen fiber-mineral composites at higher-levels of hierarchical architecture. These variations account for the distinct mechanical and chemical properties of bone versus teeth tissues. It is, therefore, important to understand the factors controlling the crystal shape and size in each of these mineralized tissues.

The apatite crystals in bone have an unusual plate-like morphology compared to their inorganically grown counterparts of prismatic or rod-like morphology. The earliest observable crystals in bone are about $40 \times 20 \times 3$ nm^3 in size, where the (100) face is the largest and the (001) face is the smallest, with (110) face of intermediate dimension.[2] It is believed that nucleation and/or growth of bone crystals is regulated by acidic functional macromolecules, such as bone sialoprotein (BSP)[3–5] and osteopontin (OPN),[6,7] as well as small acidic molecules, such as citric acid.[8,9] However, the detailed role of these molecules in bone formation is not known at the molecular level, despite many experimental studies and a few computational studies using *ab initio* cluster calculations or molecular dynamics (MD) simulations.[10–14] The development of treatments for bone diseases and disorders as well as biomimetic synthesis of bone fillers and mineral components for composite scaffolds in tissue engineering requires a knowledge of how the crystal is templated by the organic molecules. Various mechanisms of growth modulation are possible, but in each case, crystal morphology is controlled by growth

[a] *Z. Xu, Z. Wang, N. Sahai*
Department of Polymer Science, 170 University Avenue, University of Akron, Akron, Ohio 44325-3909
E-mail: zxu@uakron.edu or sahai@uakron.edu

[b] *Y. Yang*
Department of Chemistry and Biochemistry, 201 Mullica Hill Road, Rowan University, Glassboro, New Jersey 08028

[c] *D. Mkhonto*
Council for Scientific and Industrial Research, Meiring Naude Road, Brumeria 0184, South Africa

[d] *C. Shang, Z.-P. Liu*
Department of Chemistry, Key Laboratory of Computational Physical Science (Ministry of Education), Fudan University, Shanghai 200433, People's Republic China

[e] *Q. Cui*
Department of Chemistry and Theoretical Chemistry Institute, 1101 University Avenue, University of Wisconsin, Madison, Wisconsin 53706

Contract grant sponsor: NSF DMR Biomaterials (ARRA funds); Contract grant number: 0906817; Contract grant sponsor: University of Akron (N.S.); Contract grant sponsor: Rowan University (Y.Y.)

inhibition in specific crystallographic directions relative to others. We use computational approaches to explore small molecule-mediated crystal growth control of HAP nanocrystals in bone.

Many of the macromolecules, such as BSP and OPN, which are believed to control apatite growth modulation, are soluble and enriched in acidic amino acids, such as glutamic acid (Glu), aspartic acid, phosphorylated serine (Ser-OPO_3), and phosphorylated threonine.[15] These proteins are called noncollagenous acidic proteins. *In vitro* studies show that these proteins inhibit nucleation when present in solution, but promote nucleation when attached to surfaces, including that of the collagen matrix.[16–18] Phosphorylation is an energetically expensive process, so it has been suggested that the benefit must be to improve the efficiency of the proteins in controlling bone biomineralization.[15,19] Experimental studies have also displayed that some small molecules[8] and simple amino acids[11,20–24] can be used as effective regulators of HAP crystal morphology. For example, citrate, which constitutes 3–5 wt% of bone, was an effective crystal growth inhibitor of hydroxyapatite *in vitro*.[8] The plate-like morphology of HAP crystals could also be obtained *in vitro* by Glu.[11] In contrast, glycine, which has a hydrophobic side chain, did not affect morphology relative to the inorganic control and needle-like crystals were obtained.[11] The role of the acidic functional groups has been proposed as binding preferentially to the specific crystal face and inhibiting growth in the direction perpendicular to that face. However, because of a lack of face-specific information in almost all experimental studies, detailed thermodynamic and structural information controlling the growth mechanism, such as the interaction strength at specific faces and atomic-level-conformation of interaction sites, are still poorly understood. MD simulations can address this gap in our knowledge by providing the atomic level energy landscape for amino acid interactions on HAP crystal faces.

In previous simulation studies, the adhesion energy was calculated to investigate the interaction of organic molecules with the HAP (001) and (010) surfaces.[10] However, the kinetic (adsorption free energy barrier) and entropic effects on the adsorption mechanism were limited or lacking in the previous work. Furthermore, the high-charge density on HAP surfaces can result in multiple free energy minima separated by significant free energy barriers along the adsorption pathway. These barriers could trap the molecule in one of the local minima and prevent the molecule from attaining the true, lowest free energy binding conformation at the surface. Regular MD simulations are not efficient at overcoming this problem, because the technique is biased toward stable states and unstable states are poorly sampled. Another common limitation of many MD studies in the biomineralization literature is inadequate benchmarking of the applied force fields for mineral-adsorbate interactions. In the present study, we calculate the potential of mean force (PMF) for adsorption of simple organic molecules on various HAP faces using the umbrella sampling approach[25] combined with weighted histogram analysis method (WHAM).[26] We also compare our PMF results to density functional theory (DFT) coupled with a modified Poisson–Boltzmann (PB) model, which accounts for solvation in an approximate but efficient manner. Before proceeding, we provide a brief explanation of the computational methods applied in our study.

The PMF is one fundamental measure of the binding interaction including both enthalpic and entropic contributions, and is defined as the free energy profile of a chemical process as a function of a particular reaction coordinate.[27] In our study, we define the reaction coordinate as the separation between the molecule and each HAP crystal face. The PMF profile can be used to determine the energetically most favorable position, orientation, and conformation of the adsorbed amino acid near the crystal surfaces.[28] The umbrella sampling approach provides improved sampling of conformational space and avoids the pitfalls of regular MD by applying a biasing potential as the molecule moves toward the surface along the reaction coordinate. The bias in probability distributions is removed with WHAM by reweighting the probability distribution, resulting in an unbiased PMF. With an appropriate reaction coordinate, the umbrella sampling approach overcomes the problem of high-energy barriers between multiple local minima and provides the adsorption free energy landscape that includes entropic contributions. For example, Sun et al. successfully explored the interaction of various peptides with a functionalized hydrophobic surface by investigation of the PMF.[29] Pan et al. used steered MD[30] for measuring the departure force as well as the desorption free energy of glycine and Glu from the HAP (001) and (100) surfaces.[11] However, the adsorption energies obtained were unrealistically large ($\sim$60–97 kcal mol^{-1}) and the structure of interfacial water at the HAP surface was also not consistent[11] with previous spectroscopic and diffraction analyses.[31,32] More recently, adaptive umbrella sampling techniques (meta-dynamics) have been applied to various crystal growth and nucleation problems.[33–35]

One of the main goals of present work is to use the umbrella sampling approach to obtain reliable adsorption free energies and molecular conformations of water, Ser-OPO_3, and Glu on HAP surfaces. These results provide information about preferential growth directions and, ultimately, about control of crystal morphology. As one possible growth-modulating mechanism, we propose that preferential adsorption of Ser-OPO_3 and Glu on a specific crystal face, such as the (100) face in bone HAP, would inhibit growth in the perpendicular direction while allowing growth parallel to that face. As a result, the (100) face would have the largest surface area in the final crystal. Conversely, growth would be fastest in the direction perpendicular to the surface, such as the (001) face, which interacts most weakly with the adsorbing molecule, resulting in the smallest area for the (001) face. Equally or even more importantly, we aim to benchmark thoroughly the classical force fields used here for the apatite-water-organic interface by comparing our PMF results to binding energies from the coupled DFT and PB approach. This aspect of the work also sets this study apart from previous attempt to benchmark force field for mineral surface/adsorbate interactions based on gas-phase calculations[36]; due to the highly charged nature of

mineral (HAP) surface, these gas-phase calculations yield very large binding energies (~70–145 kcal mol^{-1}), making the results less useful for benchmarking. *Ab initio* or Car–Parrinello simulations can in principle be carried out. However, such calculations are usually limited to 10–50 ps for the type of system of interest here; as shown below, simulations of such time scale are orders of magnitude too short for obtaining meaningfully converged binding free energy at the water/mineral interface. Therefore, the integration of DFT and a calibrated continuum solvation (PB) model is the most effective way to calibrate surface/adsorbate interactions for our problem.

Methods

MD Simulation

In our present work, we apply MD simulations to study atomic level interactions between Ser-OPO_3 and Glu molecules with the (001) and (100) surfaces of HAP. The binding free energy or PMF is computed through umbrella sampling with WHAM using classical molecular mechanical force fields.[12,37,38] The MD simulations are performed using GROMACS 4.0 package.[39]

Bulk Crystal and Surfaces Initial Structure Preparation. Hydroxyapatite occurs in monoclinic and hexagonal crystal structures. The two structures are very similar, where Ca ions exist in two different sites, named as Ca(I) and Ca(II). Ca(I) sites occur as aligned columns along the *c* crystallographic axis and Ca(II) sites form equilateral triangles centered on the *c*-axis with the channel formation along the *c*-axis. Hydroxide groups (OH^-) are aligned within the channels formed by the Ca(II) ions. In monoclinic HAP, all of the OH^- groups in a given column point in the same direction and the OH^- alignment direction reverses in the neighboring column. The adjacent OH^- groups in the same column point in opposite directions in hexagonal HAP. In our present study, the crystal slab cleaved along the required crystallographic direction is reconstructed to obtain a dipole-moment free surface, by removing half of the atoms from the upper face of the slab to the lower face as described by Tasker.[40] It is important for the reconstruction on dipolar surface, as these surfaces have very large energy, diverging with increasing the crystal size and produce a polarizing electric field in the bulk.[39] Surface defects such as steps, terraces, kinks and so forth, are not taken into account in our model (or, indeed, in any other previously published model of HAP surfaces), because little or no experimental information is available to incorporate such defects into our model. We also do not consider chemical modifications of the crystal surface, such as hydroxylation of surface Ca^{2+} ions or protonation of surface PO_4^{3-} ions, which would render quite different surface charge distributions compared to the original ionic sites. These types of surface —Ca—OH and —PO_4H sites are known to exist on both inorganic HAP and biological HAP crystals,[41,42] and would influence electrostatic forces as well as H-bonding and solvation forces. Similarly, nonstoichiometric composition of bone HAP resulting from lattice substitutions by CO_3^{2-}, Na^+, and other ions are not considered. As for the situation with surface defects, nonideal stoichiometry and surface protonation cannot be included in the model, because there is a lack of knowledge about the density and distribution of these types of sites on specific crystal faces, and most experimental results provide only average properties.

Amino Acid Initial Structure Preparation. Zwitterionic amino acids are used in our calculations. The side chains of Ser-OPO_3 and Glu are deprotonated at the physiological condition, resulting in overall charges of −2 and −1, respectively.

Molecular Mechanics Force Field. We use the empirical potential energy function for HAP based on the rigid model developed by Hauptmann et al.[37] This force field reproduced the experimental bulk crystal parameters with high accuracy (e.g., within less than 1% deviation for a wide range of temperatures between 73 and 1273 K)[37]; therefore, the force field has been adopted extensively in various HAP-simulation studies.[11,43–45] In Hauptmann et al.'s original formulation the intermolecular interactions between the ionic groups in HAP was described as a summation of Coulombic and Born–Mayer–Huggins (BMH) potentials, respectively, for electrostatic and van der Waals interactions. In the present study, the intramolecular structures of PO_4^{3-} and OH^- are set to be rigid, and the bond lengths and bond angles are fixed to approximate the experimental measurement (e.g., P—O distance of 1.53 Å, O—P—O angle of 109.5° and O—H distance of 0.93 Å). We use the CHARMM22 force field[38] and TIP3P models[46] to treat the amino acids and the explicit water molecules, respectively, because these force fields have been applied widely and successfully in studying biological systems in the condensed phase.

The CHARMM22 force field is also used for interfacial reactions of amino acids with HAP surfaces. Van der Waals interactions are described by the classical Lennard-Jones (LJ) potential in both CHARMM22 and TIP3P force fields, whereas the HAP force field (FF) uses the BMH potential. There is no simple mixing rule between LJ and BMH terms to treat amino acid or water interactions with HAP. Therefore, the original BMH potential function for HAP is converted to CHARMM22 LJ function by optimizing the LJ parameters with respect to the BMH curves and focusing particularly in the regions of the local minima of pair-wise interatomic interactions. Once the HAP LJ parameters are obtained, the Lorentz–Berthelot mixing rule is used to obtain the parameters of LJ potential for the cross interactions between nonbonded atoms. Such a scheme to treat the interactions between amino acid and HAP crystal faces has been applied before, although no rigorous benchmarks were performed to justify its validity.[11] In our work, a set of benchmark calculations are carried out to examine systematically the performance of the optimized LJ parameters. The converted HAP LJ parameters are reported in Table 1. Point charges for different atom types used to describe the electrostatic interactions are adopted directly from Hauptmann et al.'s force field[37] (Table 1).

MD Simulation Details. To evaluate the performance of the optimized LJ parameters for HAP force field, the bulk crystal lattice parameters of the monoclinic HAP are computed with

Table 1. Partial charges and van der Waals parameters for different HAP atom types used in the simulations.

Molecule	Atom	Charge (e)	ε (kcal mol^{-1})	σ (Å)
Ca	Ca	+2.0	0.18800	3.31092
PO_4	P	+2.6	0.53500	3.56359
	O	−1.4	0.14950	3.04776
OH	O	−1.6	0.15500	3.09142
	H	+0.6	0.00025	1.33635

The charges are obtained from Hauptmann et al.'s force field.[37]

the method introduced by Hauptmann et al.[37] Specifically, a block of 8 × 4 × 3 unit cells (75.4 Å × 75.4 Å × 20.6 Å) is built as the simulation model (lattice vectors *a* and *b* are located on the *x*-*y* plane of the simulation box, and the lattice vector *c* is along the positive *z*-direction of the simulation box). At different temperatures in a range between 73 and 1273 K, we perform a set of four 300-ps NPT MD simulations at a pressure of 1 bar and a time step of 1 fs. Parrinello–Rahman[47] and Nosé–Hoover methods[48,49] are used, respectively, as the pressure and temperature coupling schemes. Periodic boundary condition (PBC) is applied in all directions. Particle mesh Ewald summation[50] is used to treat the long-range electrostatic interactions. The computed unit cell parameters at various temperatures together with the experimental values[37,51] are listed in Table 2. Interestingly, the optimized LJ parameters seem to provide even better consistency with experimental values[51] compared to the performance of the original BMH potentials (see Results and Discussion). With the same simulation setup, the standard molar lattice enthalpy of HAP crystal at room temperature is calculated based on Cruz et al.'s method.[52]

We model interactions of the (001) and (100) crystal faces of HAP with water alone and with water plus amino acids. For the (001) face, a HAP slab with dimensions of 37.7 Å × 37.7 Å × 27.5 Å (along the unit cell lattice directions) is used as the model surface, and a slab with dimensions of 37.7 Å × 34.4 Å × 32.3 Å is built as the (100) model surface. Each crystal slab is created along the direction normal to the corresponding face. Water molecules are then introduced on top of the crystal faces by using the equilibrated bulk water structure prepared previously by the NPT ensemble MD simulation. The initial *z*-dimension of the simulation box is 85 Å. In other words, a water layer of thickness more than 50 Å is added on the crystal slab in all cases to ensure the presence of a wide layer of bulk water between the crystal surface and its periodic image. This water layer thickness corresponds to 2,234 and 2,143 water molecules, respectively, for the (001) and (100) systems. The entire simulation system of 9,568 and 9,972 atoms, respectively, in the (001) and (100) systems, is kept charge-neutral by adding Na^+ counter ions in the presence of the negatively charged amino acids. Using a similar setup of simulation controlling parameters to the bulk crystal structure simulation, 10-ns isothermal-isobaric (NPT) ensemble simulations (300 K and atmospheric pressure 1 bar) with PBC in all directions are carried out for HAP-water systems. A cutoff of 14 Å is used for the separation of direct and reciprocal space. A switching scheme is applied between 12.0 and 13.0 Å for van der Waals interactions. The last 4 ns of the simulation are used as the production run for the data analysis. With the Maxwell distribution at room temperature, the initial velocities are assigned to atoms at their starting configurations.

PMF Calculations for the HAP-Water-Amino Acid System. The PMF provides the binding free energy of Ser-OPO_3 and Glu on (001) and (100) HAP faces. In practice, we calculate the free energy of desorption for moving the amino acid away from each HAP surface. The initial binding state of the amino acid on the HAP surface is obtained through an 8-ns NPT simulation with the amino acid randomly placed close to each HAP face. Subsequently, the PMF is computed with the umbrella sampling method.[25] The reaction coordinate, defined as the separation distance along the *z*-direction between the center of mass of the amino acid and the outermost Ca^{2+} ion layer at each HAP surface, extends from ~2.0–3.0 Å (the bound or adsorbed state) to ~12.0–13.0 Å (the desorbed state in the bulk water environment). Depending on the specific amino acid, ~40–60 windows are prepared from the bound state obtained from the 8-ns NPT simulation to the desorbed state, by using the PULL module implemented in GROMACS 4.0 package. The specified reaction coordinate between the adjacent windows varies by 0.05–0.5 Å depending on the sampling region and the umbrella harmonic potential force constant correspondingly ranges from 150,000 to 1000 kJ mol^{-1} nm^{-2} to ensure sufficient overlapping of conformational space. A series of biased simulations were then performed with various defined separation values spanning the entire range of interest on the surface to construct the PMF as a function of the distance. A 4-ns simulation is carried out for each window (160–240 ns for each of the PMF curves). The first 1 ns is used for system equilibration and the last 3 ns of the simulation are treated as the production run. The production runs are used to obtain the unbiased PMF for desorption using WHAM.[26] Finally, we assume that the resulting PMF reaches a plateau when the amino acid has moved into the water bulk solution phase. The region 1.0–1.3 nm away from the surface, where the amino acid is considered to be in the bulk phase, was used as a baseline to superimpose the PMFs. The free energy difference between the desorbed state (amino acid is in the bulk water) and the bound (adsorbed) state obtained from the PMF curve is defined as the binding or adsorption free energy in the following discussions. Usually, the adsorbates (such as

Table 2. Simulated and experimental HAP unit cell parameters[37,51] at different temperatures.

Temperature (K)	Type	*a* (Å)	*b* (Å)	*c* (Å)	α (°)	β (°)	γ (°)
73	Exp.	9.377	18.754	6.881	90.0	90.0	120.0
	Sim.	9.385	18.770	6.943	90.0	90.0	120.0
300	Exp.	9.404	18.808	6.901	90.0	90.0	120.0
	Sim.	9.397	18.794	6.946	90.0	90.0	120.0
600	Exp.	9.441	18.882	6.928	90.0	90.0	120.0
	Sim.	9.418	18.836	6.953	90.0	90.0	120.0
1273	Exp.	9.523	19.046	6.987	90.0	90.0	120.0
	Sim.	9.497	18.995	6.984	90.0	90.0	120.0

surfactant and peptide) may potentially bind to a surface at different sites corresponding to various local binding free energy minima. In order to investigate the reliability of umbrella sampling simulation, we have also tested a different scheme to construct a series of initial structures, where the free energy calculations started with the initial structure of the amino acid in desorbed state. The initial structure for the next window toward the surface was obtained from the last sampling simulation. Therefore, the umbrella sampling simulations were performed subsequently until the amino acid approaches the surface with a separation of ~2–3 Å. We compared the free energies obtained from the two schemes and observed similar characteristics of the PMF profiles.

DFT-PB Calculations

All DFT-PB calculations are performed using SIESTA[53,54] where optimized double-ζ plus polarization numerical atomic orbital basis sets[55] are utilized along with the Troullier–Martins norm-conserving pseudopotentials.[56] The exchange correlation functional is utilized at the generalized gradient approximation level proposed by Perdew, Burke, and Ernzerhof.[57] The cutoff for the real space grid is set as 150 Ry. The limited memory-Broyden–Fletcher–Goldfarb–Shanno method is used for geometry relaxation until the maximal forces on each relaxed atom were less than 0.1 eV $Å^{-1}$. Long-range electrostatic solvation in aqueous surroundings is taken into account by using a periodic continuum solvation model based on the modified PB equation. For the implementation of the numerical PB solver in periodic slab calculations, we utilize a sixth-order finite-difference scheme to discretize partial differential equations with PBC, which is solved numerically in the self-consistent loop by modifying SIESTA code.[58,59] More details of the methodology has been addressed in the recent publication,[60] in which the calculation accuracy has been benchmarked for a number of static and dynamic electrochemical properties, including the potential of zero charge, the differential capacitance and the Tafel curve. The periodic continuum solvation model represented by a modified PB equation has been extensively utilized to investigate the adsorption of large ion/molecule from solution to various surfaces[58,59,61,62] and provide the valuable information of adsorption free energy at the solid/water interface, such as formic acid at Pt/water interface[58] and the water adsorption on titania[62] and on RuO_2 (110) surface in aqueous surroundings.[59] Explicit solvation must be considered to account for specific interactions that are expected between charged amino acids or the ionic HAP surfaces and water in the first solvation shell. Inclusion of explicit water molecules for interfacial solvation can better describe the structural characteristics of the water layer between the amino acids and the surface, which the implicit solvation model cannot provide. We include explicit waters in the first solvation shell, where the initial structures were obtained from the PMF simulations. Therefore, 34 and 16 water molecules, respectively, are used to represent the solvation shell of Ser-OPO_3 and Glu molecules in solution.

The adsorption free energy of a molecule A on HAP (A/HAP) from DFT-PB calculation is calculated by $G_{ad} = G_{A/HAP} + nG_{H2O} - G_A - G_{HAP}$, where G_X is the free energy of X in solution and n is the number of explicit water molecules that are required to balance the reaction stoichiometry. For the solid states before and after adsorption, G_{HAP} and $G_{A/HAP}$, the DFT-PB total energy is a good approximation of the free energy. For G_{H2O}, the experimental value at the standard state is utilized, which is 0.57 eV lower than the DFT-PB total energy. The solvation free energy of A, G_A, is calculated by immersing A into an explicit water molecule network that is further surrounded by implicit solvation (PB model). Although we realize that the DFT-PB approach also has several approximations, especially regarding the entropic factors associated with the adsorbate and interfacial water, this approach is qualitatively different from gas-phase type of DFT calculations and the DFT-PB model has been calibrated and successfully utilized for solid–liquid interface systems in electro-/photocatalysis studies.[62,63]

The (100) surface of HAP is modeled by a (1 × 2) unit cell (19.13 × 13.96 Å). Only Γ point is used to sample the first Brillouin zone. The (100) slab contains six phosphate layers (12.5 Å thick) with the middle two layers fixed at the bulk position. Adsorption is modeled by adding the amino acid molecule on both sides of the slab. Explicit charges are added to the system for ionic molecules, Ser-OPO_3 and Glu, while the balancing background charge is distributed according to the PB equation in continuum solvation region. Eight Ca^{2+} ions and four PO_4^{3-} groups are exposed on the upper and lower surfaces of the (100) slab, which is covered by 28 water molecules as the first water solvation shell for each side of the slab.

Results and Discussion

Verification of LJ parameters of the modified HAP force field

As stated in the Methods section, the original HAP BMH potential function developed by Hauptmann et al.[37] is converted to the LJ potential under CHARMM22 force field in order to treat the cross interactions at the interface between the amino acid and the HAP crystal using the established Lorentz–Berthelot mixing rule. The performance of the optimized LJ parameters for the HAP force field is evaluated first by calculating the bulk crystal lattice parameters. Interestingly, our optimized LJ parameters seem to provide even better consistency to the experimental values as compared to the original BMH potentials. For example, the average deviation for lattice parameters, *a, b*, and *c*, at four different temperatures (73, 300, 600, and 1273 K) is 0.28% based on our LJ parameters, which is smaller than the 0.42% deviation from Hauptmann et al.'s results. For room temperature, at which the subsequent HAP-water and HAP-water-residue simulations are performed, the LJ parameters provide an average deviation of 0.27%, compared to the larger deviation of 0.39% with the BMH parameters.

In addition to the reproduction of the HAP bulk lattice structural parameters, two other crystal properties are computed as additional evaluation of the accuracy of our LJ parameters. The standard molar lattice enthalpy of HAP crystal

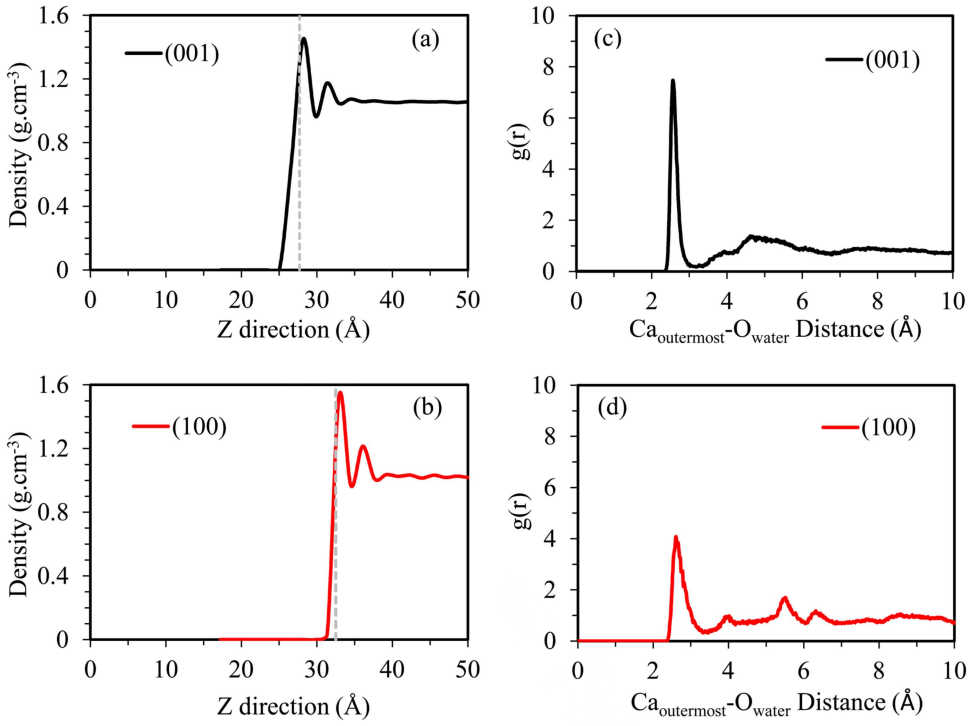

Figure 1. Water density distributions (left panel) and radial distribution functions (right panel) of water molecule around the outermost Ca^{2+} ions on the HAP (001) (upper panel) and (100) faces (lower panel). As a reference, in the water density profiles, the outermost Ca^{2+} ions are at 27.7 and 32.5 Å along the *z* direction, respectively, for HAP (001) and (100) surfaces. [Color figure can be viewed in the online issue, which is available at wileyonlinelibrary.com.]

at room temperature, based on Cruz et al.'s method,[52] is computed to be $-34{,}077.40$ kJ mol^{-1}, which is comparable to the available experimental value of $-34{,}183 \pm 134$ kJ mol^{-1} available for the hexagonal phase. Furthermore, the computed isobaric thermal expansively coefficient of 1.535×10^{-5} K^{-1} is also consistent with a previous MD calculation result of 1.82×10^{-5} K^{-1}.[52] These results indicate the accuracy of the converted LJ parameters to treat the HAP crystal structure. Because of the large ionic charges in the HAP crystal, a good simulation of bulk crystal structure and parameters should have the ability to generate an accurate electrostatic potential, which is critical to investigate accurately the interactions of water and/or organic molecule with crystal surfaces.

HAP-Water Interactions

In the original HAP force field of Hauptmann et al.,[37] the interactions of HAP with organic or water molecules were not taken into account, and although the force field has been combined with various molecular mechanical force fields, for example, CHARMM[38] and OPLS[64] for organics and SPC[65] for water and so forth, the performance of such a "mixing" has not been examined in detail. In our present work, therefore, we explore the interactions between HAP faces and water before proceeding to adsorption of amino acids. We focus particularly on the structure of water structures at the HAP (001) and (100) faces. MD simulations of 10 ns ensure that the water structure is fully equilibrated as indicated by the convergence of the system potential energy. Consistent with our expectation, water molecules form favorable interactions on both HAP faces independent of the surface because of strong ion-dipole interactions. The water density profile on both HAP faces shows two significantly structured water layers (Figs. 1a and 1b), consistent with previous experimental studies.[31,32] Specifically, for the HAP (001) face, the first peak along the density distribution curves occurs at ~0.3 Å above the outermost Ca^{2+} ions and the second peak is seen at ~3.3 Å. The first stable water layer, with a density of 1.45 g cm^{-3}, is formed due to strong interactions between water molecules and HAP surface ions. These water molecules directly coordinate to the outermost Ca^{2+} and are also able to form direct interactions with OH^- and PO_4^{3-} groups, which are slightly below the top Ca^{2+} layer. The second water layer interacts mainly with the outermost Ca^{2+} ions and water molecules in the first layer, resulting in a density of 1.17 g cm^{-3}. The radial distribution function of water around the outermost Ca^{2+} ions showed that four water molecules form direct interactions with each of the outermost Ca^{2+} ions with an average Ca—O distance of 2.58 Å (Fig. 1c).

On the HAP (100) face, we again observe two water layers, with the maximum density peak located at ~0.5 and ~3.5 Å from the surface (Fig. 1b). The density of the first water layer is ~1.53 g cm^{-3}. The water molecules interact directly with the outermost Ca^{2+}, the underlying Ca^{2+} layer, and oxygen atoms of PO_4^{3-} groups at the surface, where one water molecule is observed to form two hydrogen bonds with two adjacent PO_4^{3-} groups. Three water molecules are within the first coordination shell of each outermost Ca^{2+} ion, at an average

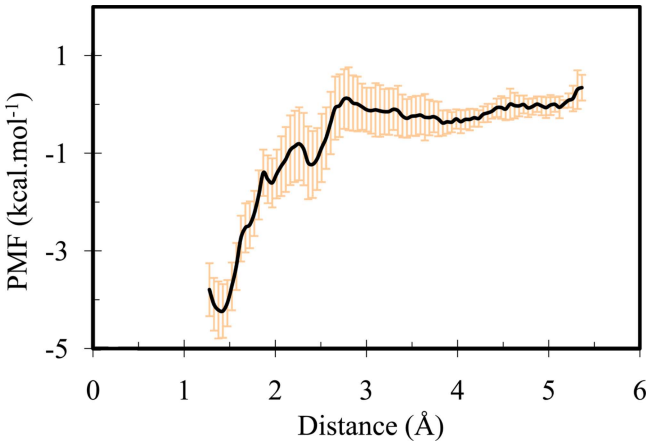

Figure 2. Free energy profile for adsorption of a single water molecule on the HAP (001) face. The error bars in the PMF were estimated by calculating the 95% confidence interval of the mean value by dividing the simulation trajectory into four blocks. [Color figure can be viewed in the online issue, which is available at wileyonlinelibrary.com.]

Ca—O distance of 2.60 Å (Fig. 1d). Water molecules also form direct interactions with surface ions by positioning just above the ions, which helps form the second stable water layer where the water density is 1.21 g cm^{-3}. Furthermore, the (100) face is atomically smoother than the (001) face, so water molecules are observed to form more extended hydrogen bond networks on the former face.

Our results for the interfacial water structure are consistent with experimental results. Synchrotron-based specular X-ray reflectivity crystal truncation rod studies of interfacial water at the (100) face of fluorapatite showed two distinct water layers.[31] The two structured water layers extended up to ~4.2 Å from the surface. These results were later confirmed by Pareek et al.[32] using grazing incidence X-ray diffraction. Using the HAP force field developed by Hauptmann, OPLS-AA force field for Glu and Gly and SPC water model, Pan et al.[11] studied the structure of water on HAP (001) and (100) faces. In contrast to our results and to the experiments cited above, Pan et al. found 4–5 water layers with a total thickness of 1 nm on both HAP (001) and (100) faces. Furthermore, a highly condensed water layer with a density of nearly 3 g cm^{-3} was obtained on the (001), and ascribed to the formation of an ice-like structure. A high-density water structure of ~3.5 times the density of bulk water was also obtained in the simulation work by Zahn and Hochrein,[43] who combined BMH potential for HAP and TIP3P water model but with OPLS force field for water-HAP interaction. Unfortunately, no explanation was provided in either study for these high-density water layers extending up to 1 nm away from the surface. We believe that the high-density water may be a result of improper accounting of cross-terms in the force fields for intermolecular interactions at the crystal-water interface, which make their calculations less convincing as benchmarks for further simulations of HAP-water-organic interactions.

In order to further investigate the reliability of our HAP-water interaction force field, we have also calculated the adsorption free energy of a single water molecule using the PMF approach (Fig. 2) and compared the result to the energy obtained from *ab initio* DFT-PB calculations. The PMF adsorption energy is −4.2 kcal mol^{-1}, which is close to the value of −5.1 kcal mol^{-1} obtained from DFT-PB (Table 3). The PMF adsorption energy is also comparable to the value of 0.8 kcal $mol^{-1}$for H_2O molecule on calcite ($CaCO_3$) reported by Parker,[66,67] who also used the umbrella sampling/WHAM method (Table 3).

HAP-Ser-OPO_3 Interactions

Consistent with chemical intuition, the interactions between the amino acids and different faces of HAP strongly relate to the structure of the crystal surfaces. As seen in Figure 3, Ser-OPO_3 shows distinct PMF profiles on the HAP (001) and (100) faces. Moving away from the surface along the desorption pathway, the free energy profile oscillates and approaches zero beyond 10 Å from the surface, where the amino acid is effectively in bulk water. When the Ser-OPO_3 is close to the (001) face, the PMF profile displays one free energy minimum of −4.5 kcal mol^{-1} at ~3.6 Å from the surface. The conformation at this position indicates interactions of Ser-OPO_3 with the structured water layers between the molecule and the surface (Fig. 4a). The Ser-OPO_3 is oriented parallel to the surface with —NH_3^+ penetrating into the first water layer. However, we do not observe any direct interactions between Ser-OPO_3 and surface ions in our simulation. We pay special attention in the region below 3.6 Å, where many additional sampling windows from 2.0 to 4.0 Å are carefully investigated with different initial structures, to ensure that we sample accurately the conformational space. The same results as shown above are obtained without further adsorption of the amino acid at closer distance on the surface. Thus, it appears that the Ser-OPO_3 molecule does not significantly penetrate the water layer on the (001) surface. Similar behavior has been reported in crystal truncation rod experiments and MD simulations of glycine at the (104) face of calcite.[68]

The PMF curve on the (100) face is clearly different from that on (001) face. Three significant local minima of −8.1, −9.5, and −9.8 kcal mol^{-1}, respectively, are obtained at 3.8, 3.0, and 2.2 Å from the surface [points (b), (c), and (d) in Fig. 3]. The corresponding structures are shown in Figure 4. The adsorption energy obtained from the DFT-PB calculation is −12.2 kcal mol^{-1} for the structure corresponding to the deepest PMF energy minimum [point (d) in Fig. 3 and structure in Fig. 4d]. Evidently, Ser-OPO_3 is able to penetrate the interfacial water layer, on the (100) face, thus binding more closely and

Table 3. Benchmarking adsorption free energies (kcal mol^{-1}) of water on HAP (001) and of small molecules on HAP (100) obtained from PMF by umbrella sampling/WHAM method by comparison with results of DFT-PB calculations.

Calculation method	Small molecule		
	Water/(001)	Ser-OPO_3/(100)	Glu/(100)
DFT-PB	−5.1	−12.2	−7.5
PMF	−4.2	−9.8	−8.2

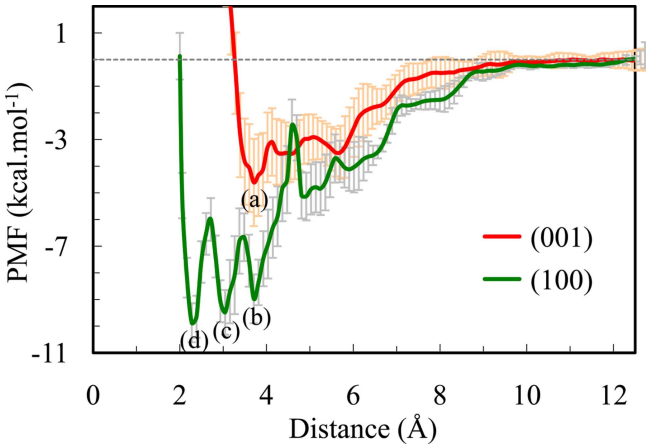

Figure 3. Free energy profile of Ser-OPO_3 adsorption on HAP (001) and (100) faces. The points (a)–(d) correspond to the structures presented in Figure 4. Explanation for error bars as provided in Figure 2 caption. [Color figure can be viewed in the online issue, which is available at wileyonlinelibrary.com.]

with much stronger interactions than at the (001) face (water molecules on (100) face in Figures 3b–3d are omitted for clarity of illustration). The Ser-OPO_3 molecule has to cross two free energy barriers with heights of 2.6 and 4.6 kcal mol^{-1}, which separate the three energy minima, to transfer from the bulk solution phase to the surface. Each free energy barrier represents a separate adsorption/desorption conformation. These free energy barriers may trap Ser-OPO_3 in a local minimum. Such multiple energy traps have also been observed in other simulation studies[28,69,70] and atomic force microscopy experiments. It is these kinds of closely spaced minima that may not be properly sampled by traditional MD simulations and this is why umbrella sampling and WHAM method is critical for reliable results.

The structures corresponding to the three free energy minima are shown in Figure 4. At 3.8 Å distance from the surface, the molecule "stands up" on the surface with the three oxygen atoms of $—OPO_3^{2-}$ group directly interacting with the outermost Ca^{2+} ions (Fig. 4b). As the separation decreases, the $—COO^-$ group on the alpha carbon approaches closer to the surface (Fig. 4c). In these two steps, the Ser-OPO_3 molecule completely crosses the interfacial water layer. Finally, the molecule lies parallel to the (100) surface with the $—COO^-$ group and two oxygen atoms of the $—OPO_3^{2-}$ group pointing to the surface (Fig. 4d). The fourth oxygen atom of the $—OPO_3^{2-}$

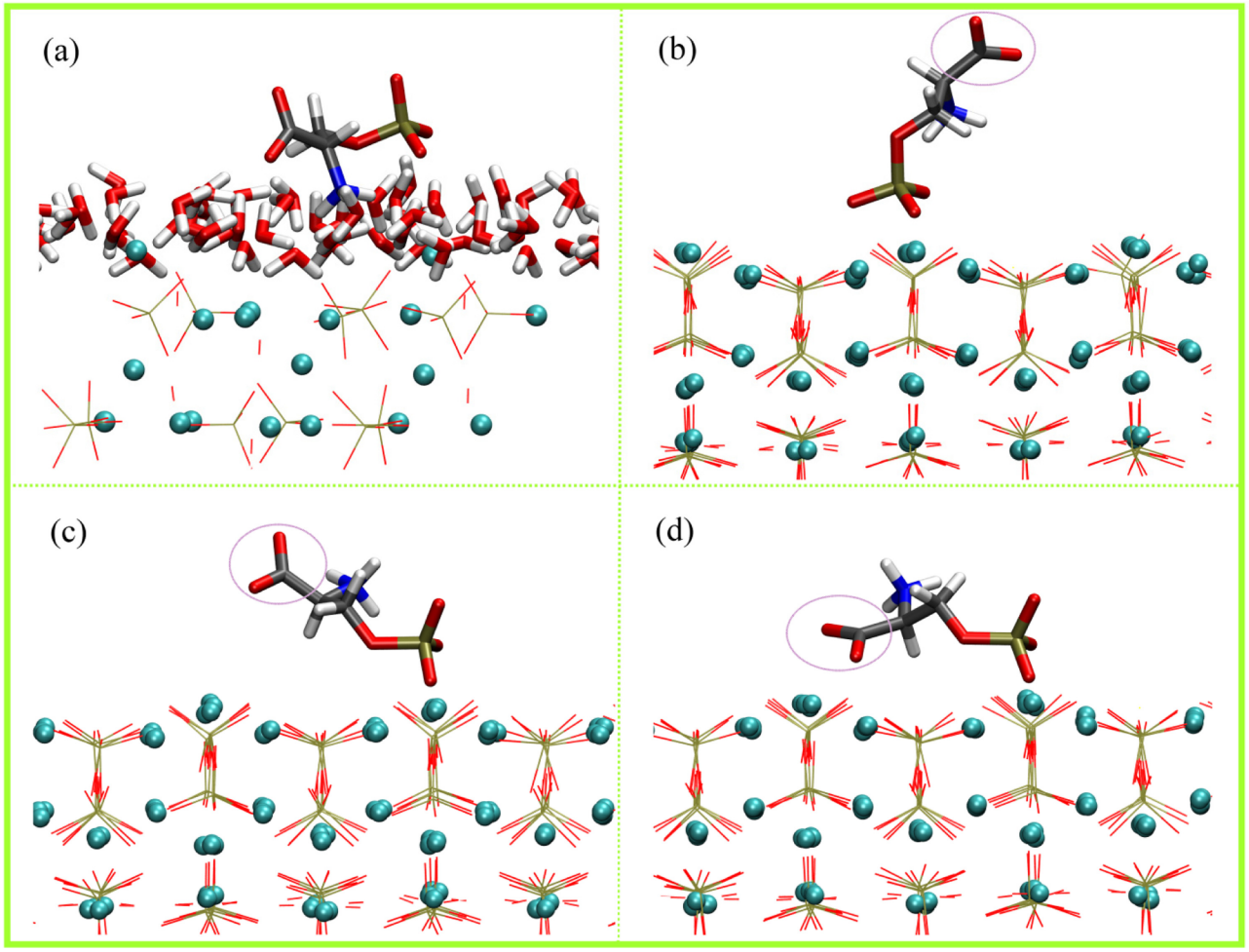

Figure 4. Representative snapshots of Ser-OPO_3 at the HAP (001) face (a) and at the (100) face (b–d) corresponding to points (a)–(d) in Figure 3. Ser-OPO_3 forms direct interactions with the (100) surface, but interacts indirectly with (001) through stable interfacial water layers. The stable "sandwiched" water layers between Ser-OPO_3 and the (001) surface are shown in Figure 4(a); the other water molecules in that structure and water in structures (b)–(d) are not shown for clarity. Legend: H = white; C = grey; N = dark blue; O = red; P = tan; Ca = cyan spheres.

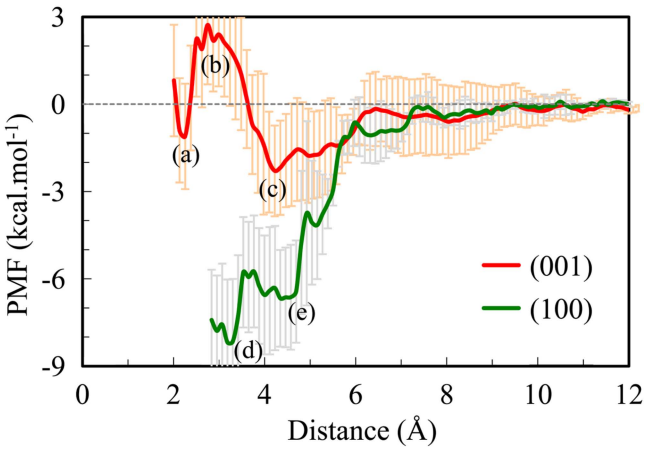

Figure 5. Free energy profile of Glu adsorption on HAP (001) and (100) faces. The points (a)–(e) correspond to the structures presented in Figure 6. Explanation for error bars as provided in Figure 2 caption. [Color figure can be viewed in the online issue, which is available at wileyonlinelibrary.com.]

group points away from the surface. The free energy barrier between these minima arises, because of a delicate force balance between the interactions of the surface with the $—OPO_3^{2-}$ group of phosphoserine and with the $—COO^-$ group of the alpha carbon. As Ser-OPO_3 approaches the surface, the increasing interaction of of the $—COO^-$ group with the surface results in a slightly more stable configuration, which however, partially breaks up the already formed bonds between the $—OPO_3^{2-}$ group and the surface ions. This energetic trade-off produces the free energy barrier.

HAP-Glu Interactions

The free energy profiles for interactions of Glu with HAP surfaces are shown in Figure 5. The PMF calculation on the (001) face indicates two free energy minima of −1.3 and −2.2 kcal mol^{-1} located at 2.2 and 4.2 Å from the surface, respectively [points (a) and (c) in Fig. 5]. The former minimum corresponds to direct binding of Glu with ions at the (001) face (Fig. 6a), and the second minimum refers to a conformation in which Glu interacts with interfacial water layers at the (001) surface (Fig. 6c). A barrier with a height of 4.8 kcal mol^{-1} separates the two minima, where the reference energy is the remote minimum from the surface.

At the binding configuration closest to the surface, Glu adsorbs directly to the (001) face by lying parallel to the surface (Fig. 6a). The $—COO^-$ group of the side chain binds with the H of an OH^- group in a bidentate mode at an average $O_{Glu\ sidechain}$-$H_{hydroxide}$ distances of 2.43 and 2.98 Å, respectively. The $—COO^-$ group of the alpha carbon forms a stable electrostatic interaction with an outermost Ca^{2+} ion in a monodentate mode at a $O_{Glu\ mainchain}$-Ca distance of 2.46 Å. The alpha carbon $—NH_3^+$ group does not form direct interactions with (001) surface.

In the transition state separating the two energy minima, similar to the direct binding state, the sidechain $—COO^-$ still forms a bidentate interaction with the OH^- group at the HAP surface (Fig. 6b). The amine group forms a stable intramolecular hydrogen bond with the side chain carboxyl group at an average H_{amine}-$O_{sidechain}$ distance of ∼1.7 Å, and the main chain $—COO^-$ points away from the HAP surface.

At the global minimum of −2.2 kcal mol^{-1} where Glu lies 4.2 Å from the surface, the molecule is oriented parallel to the HAP surface with two $—COO^-$ groups pointing toward the surface and the $—NH_3^+$ group pointing away from the surface (Fig. 6c). However, Glu does not form any direct interaction with surface ions in this configuration and ∼1–2 water layers separate Glu and the (001) surface. Thus, Glu prefers to bind with the interfacial water layers at the (001) surface instead of interacting directly with the HAP surface ions.

The PMF curve for Glu at the (100) surface is significantly different from that on (001) face (Fig. 5) and corresponding structures are shown in Figures 6d and 6e. Two free energy minima of −8.2 and −6.5 kcal mol^{-1} are obtained at 3.2 and 4.7 Å from the surface, respectively (Fig. 5). The DFT-PB adsorption energy for the structure in Figure 6d is −7.5 kcal mol^{-1}, in close agreement with the PMF value. The positions of the free energy minima relate to the arrangement of surface ions and the adsorbed water layer. The 1 kcal mol^{-1} barrier separating the two minima is smaller than in the case of the (001) face, where the energy reference is the remote minimum from the surface. The barrier height is comparable to thermal fluctuations at room temperature (∼0.6 kcal mol^{-1}), indicating that Glu is capable of kinetically overcoming the free energy barrier and of forming direct interactions with ions on the (100) face.

Due to the greater exposure of surface ions on (100) face than that on (001) face to the adsorbing Glu and bulk water, Glu can form more direct interactions with surface ions. Thus, in the global energy minimum conformation, Glu lies parallel on the (100) face with charged functional groups pointing toward the crystal surface and forms four stable, direct interactions with the surface (Fig. 6d). Each $—COO^-$ group (one from the alpha carbon and the other from the side chain) binds with a surface Ca^{2+} ion in a monodentate mode. The average O_{Glu}-Ca distances are 2.52 Å (from main chain $—COO^-$) and 2.50 Å (from side chain $—COO^-$). The $—NH_3^+$ group interacts strongly with an oxygen atom of an outermost surface PO_4^{3-} group with an average H_{amine}-$O_{phosphate}$ distance of ∼1.6 Å. This interaction is in contrast to adsorption at the (001) face, where the amine group does not form any direct interaction with HAP surface ions. A stable intramolecular hydrogen bond also forms at (100), where the converged average H_{amine}-$O_{Glu\ sidechain}$ distance is ∼1.7 Å, similar to the result for the (001) face. At the second energy minimum, Glu is located at ∼4.7 Å from the surface. The molecule is still parallel to the (100) face, but does not bind directly with any surface ions (Fig. 6e).

Implications for Crystal Growth and Morphology Control

One of the main goals of our study was to examine whether the unusual plate-like morphology of bone nanocrystals can be explained by preferential adsorption of small molecules such as amino acids on specific crystal faces of HAP. We recognize that this may be only one of many potential mechanisms

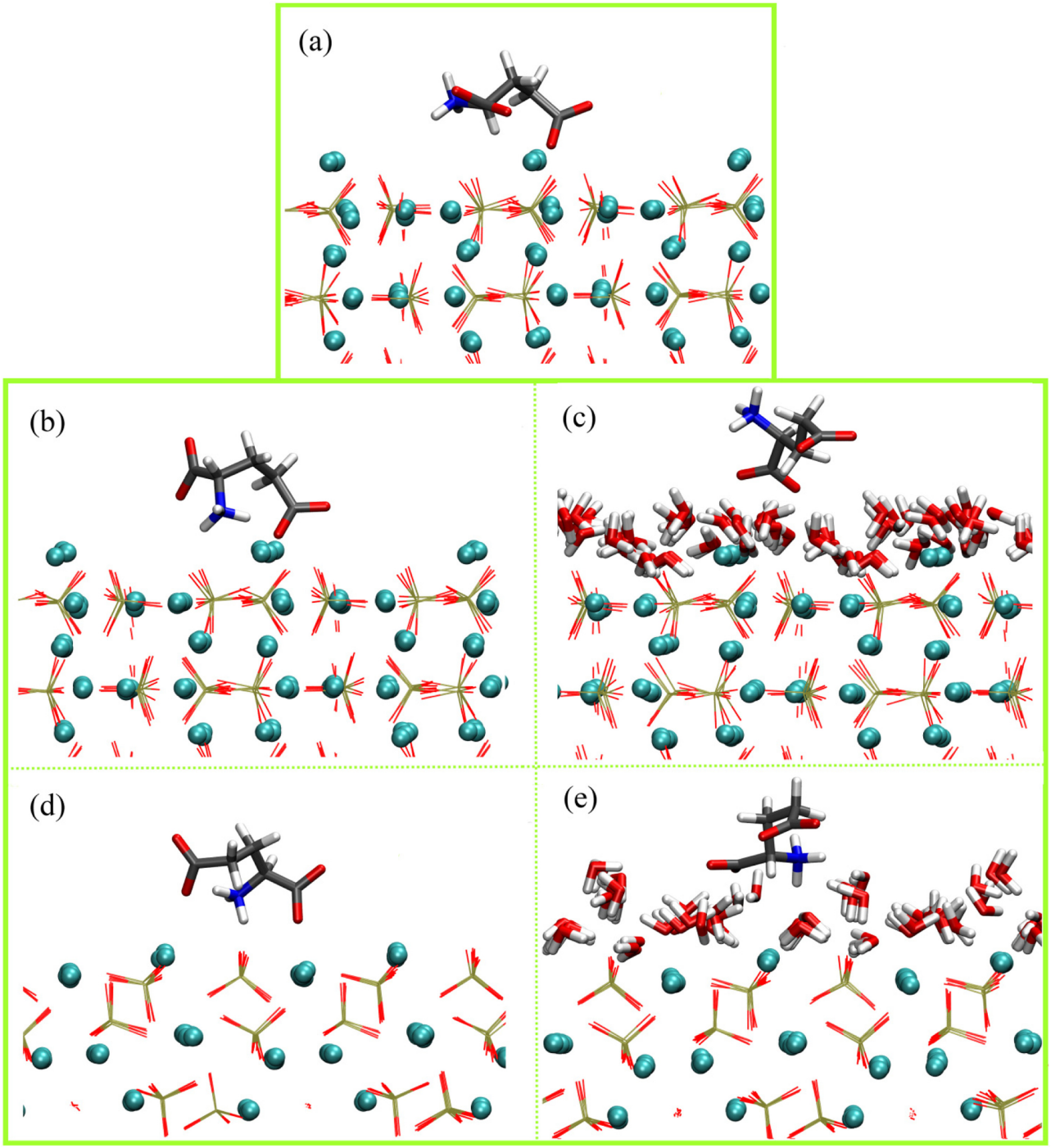

Figure 6. Representative snapshots of Glu at the HAP (001) face (a–c) and at the (100) face (d, e) corresponding to points (a)–(e) in Figure 5. Water molecules are shown in the same way as in Figure 4. Legend: H = white; C = grey; N = dark blue; O = red; P = tan; Ca = cyan spheres.

controlling HAP crystal growth *in vivo* during bone biominerlization. MD simulations with umbrella sampling[25] and WHAM[26] suggest that both Ser-OPO_3 and Glu adsorb more strongly on the HAP (100) face than on the (001) face. Thus, growth rate along the *a*-crystallographic axis should be slower than in the direction along the *c*-crystallographic axis. Thus, the crystal can grow parallel to the (100) face but growth is limited parallel to the (001) face, resulting in a plate-like crystal morphology with greater surface area for the (100) face compared to the (001). These inferences are in good agreement with the observed morphology of bone nanocrystals.[2] The relative strengths of adsorption are related in detail to the conformation of the adsorbed molecule at each face, which are revealed here through sufficient sampling of the structures. Three low-energy conformations of the Ser-OPO_3 molecule on the (100) face are identified, where both the —OPO_3^{2-} and the —COO^- functional groups interact with the Ca^{2+} ions of the crystal surface. This special conformation on the surface finally

determines the interaction and kinetics of adsorption, and thus, the growth mechanism of the crystal. In contrast, only one minimum-energy conformation is found on the (001) surface and, surprisingly, it is the $-NH_3^+$ functional group of the amino acid that interacts via H-bonds with the PO_4^{3-} groups on the crystal surface. Also, interactions of both amino acids at the (001) face occur with the interfacial water layer and not directly with the HAP surface ions. Our results suggest that preferential adsorption on specific crystal faces of even small molecules such as amino acids or citrate may be sufficient to modulate the growth and crystal morphology of plate-like HAP nanocrystals in bone.

The stronger binding of Ser-OPO_3 versus Glu on the (100) face of HAP suggests that phosphorylated proteins may, indeed, be more efficient in controlling bone biomineralization. Similar concepts may also apply to phosphorylated proteins which control biomineralization of teeth and salivary proteins which inhibit HAP nucleation. Thus, phosphorylated histatins were found to bind more strongly to HAP than their unphosphorylated analogs.[71] We recognize that in a protein or peptide, the alpha $-COO^-$ and $-NH_3^+$ groups would not be available and only the side chain groups would be involved in binding to HAP. However, the results provide a conceptual basis for suggesting that crystal growth and morphology modulation of bone nanocrystals may be controlled by similar kinds of interactions involving noncollagenous acidic proteins, such as BSP or OPN, or small molecules, such as citrate.

Importance of Benchmarking Results of Classical Force Field MD Simulations for Biomineralization Studies

A major contribution of the present work is to highlight the importance of careful benchmarking of classical force fields, especially for processes, such as biomineralization, that involve organic-water–mineral interfacial interactions. Furthermore, our study shows that a reliable calculation of the binding PMF, which features multiple minima separated by barriers, requires the use of computational methods such as umbrella sampling and WHAM for relatively long-period simulations (~160–240 ns for one PMF curve), which has not been the norm in most previous computational studies of biomineralization. For example, Pan et al.[11] applied Jarzynski's equality for PMF calculation from steered MD simulations. In those calculations, external forces are applied to the adsorbing glycine or glutamate molecules on the HAP (001) and (100) surfaces. The adsorption free energies obtained for Glu were ~400 kJ mol^{-1} (~96 kcal mol^{-1}) and ~300 kJ mol^{-1} (72 kcal mol^{-1}), respectively, on the HAP (001) surface and (100) surface. Thus, the results of Pan et al.[11] suggested that Glu adsorbs more strongly to the (001) face than the (100) face. If this were the case, then the (001) face should have a larger surface area than the (100), which is not consistent with observation for bone nanocrystals.[2] Furthermore, the order of magnitude of the adsorption energy for Glu was much larger than the values we obtained of ~2 and ~8 kcal mol^{-1}, respectively, for the two faces. In Pan et al.'s[11] simulation of Glu approaching the (001) and (100) surfaces from bulk solution, the PMF profile is smooth, showing a monotonous decrease. The results of our present umbrella sampling approach indicate structural nuances of the free energy landscape which were not observed using Jarzynski's equality from steered MD simulations.[11] The large error fluctuations of 24 and 14 kcal mol^{-1} for (100) and (001) surface, respectively, may have prevented the identification of structural details.

Another key factor is proper modeling of the interfacial water layer at the biomineral surface. The adsorbed water layer has proved to play a key role in obtaining reliable adsorption free energies.[28,67] In complex systems, the free energy calculation from steered MD method suffers from the relaxation problems and longer simulation time (more trajectories) is needed to produce the reliable PMFs.[72] This fact may explain the unrealistic interfacial water structure obtained by Pan et al. In another study, Zahn and Hochrein[43] mixed the TIP3P water model with OPLS force field for HAP to simulate water interaction at HAP (001) surface and, again, the water density obtained was not consistent with experimental results. Finally, we note that in previous attempts to benchmark adsorption energies obtained from classical force field MD simulations with energies from DFT calculations, solvation effects were not included, and again, the binding energies obtained were unrealistically large, ~100 of kcal mol^{-1}.[36,73] Most biominerals are ionic solids, and as demonstrated by our DFT-PB benchmarking, it is critical to include solvation to model the interactions between charged or zwitterionic organic molecules and the highly charged biomineral surfaces. Importantly, although there are also limitations in the DFT functional and the PB-based solvation model, the DFT-PB approach is qualitatively different from gas-phase type of benchmark calculations and gives binding energies of the same order of magnitude as the umbrella sampling calculations.

Conclusions

The main goals of the study are to highlight, in the biomineralization field, the importance of careful benchmarking of force fields especially for interfacial reactions and to apply modeling techniques that can accurately capture subtle structural changes of the adsorbate at the interface. We have achieved this goal by using the amino acid-HAP-water system to address how amino acids may influence the direct crystal morphology from needle-like to plate-like, by preferential amino acid adsorption on specific crystal faces. In particular, we show that careful benchmarking of classical force fields for organic-water–mineral interfacial reactions and long simulation times (~100 ns) are necessary to obtain reliable results to model adsorption at HAP surfaces, or indeed, any organic–inorganic-water interface. We benchmark our results to those from *ab initio* DFT-PB calculations, to previously published spectroscopy and diffraction results of interfacial water on fluorapatite. Futhermore, techniques such as umbrella sampling and two-dimensional metadynamics[74] provide a more detailed description of structures along the free energy surface. We also show that the preferential adsorption of small molecules, such as phosphoserine and glutamate, in specific crystallographic directions is sufficient to explain the observed plate-like

morphology of bone nanocrystals, although we do not claim that this is the only possible mechanism or the pathway controlling *in vivo* bone growth.

Acknowledgment

The authors thank Weilong Zhao for interesting discussions. We are grateful for the use of Ohio Supercomputer Center at The Ohio State University and the Condor High Throughput Computing at the University of Wisconsin-Madison.

Keywords: PMF · free energy · umbrella sampling · crystal growth · apatite · bone

How to cite this article: Z. Xu, Y. Yang, Z. Wang, D. Mkhonto, C. Shang, Z.-P. Liu, Q. Cui, N. Sahai. *J. Comput. Chem.* **2014**, *35*, 70–81. DOI: 10.1002/jcc.23474

[1] L. Knott, A. J. Bailey, *Bone* **1998**, *22*, 181.
[2] B. R. Heywood, N. H. Sparks, R. P. Shellis, S. Weiner, S. Mann, *Connect. Tissue Res.* **1990**, *25*, 103.
[3] A. L. Boskey, *Ann. N. Y. Acad. Sci.* **1995**, *760*, 249.
[4] J. K. Chen, H. S. Shapiro, J. L. Wrana, S. Reimers, J. N. Heersche, J. Sodek, *Matrix* **1991**, *11*, 133.
[5] N. L. Harris, K. R. Rattray, C. E. Tye, T. M. Underhill, M. J. Somerman, J. A. D'Errico, A. F. Chambers, G. K. Hunter, H. A. Goldberg, *Bone* **2000**, *27*, 795.
[6] J. Chen, K. Singh, B. B. Mukherjee, J. Sodek, *Matrix* **1993**, *13*, 113.
[7] G. K. Hunter, C. L. Kyle, H. A. Goldberg, *Biochem. J.* **1994**, *300*, 723.
[8] Y. Y. R. Hu, A. Rawal, K. Schmidt-Rohr, *Proc. Natl. Acad. Sci.* **2010**, *107*, 22425.
[9] B. Xie, G. H. Nancollas, *Proc. Natl. Acad. Sci.* **2010**, *107*, 22369.
[10] N. H. de Leeuw, J. A. L. Rabone, *CrystEngComm* **2007**, *9*, 1178.
[11] H. Pan, J. Tao, X. Xu, R. Tang, *Langmuir* **2007**, *23*, 8972.
[12] Y. Yang, Q. Cui, N. Sahai, *Langmuir* **2010**, *26*, 9848.
[13] N. Sahai, *Am. J. Sci.* **2005**, *305*, 661.
[14] Y. Yang, D. Mkhonto, Q. Cui, N. Sahai, *Cells Tissues Organs* **2011**, *194*, 182.
[15] A. George, A. Veis, *Chem. Rev.* **2008**, *108*, 4670.
[16] P. A. Price, D. Toroian, J. E. Lim, *J. Biol. Chem.* **2009**, *284*, 17092.
[17] M. J. Olszta, X. Cheng, S. S. Jee, R. Kumar, Y.-Y. Kim, M. J. Kaufman, E. P. Douglas, L. B. Gower, *Mater. Sci. Eng. R* **2007**, *58*, 77.
[18] D. Toroian, J. E. Lim, P. A. Price, *J. Biol. Chem.* **2007**, *282*, 22437.
[19] M. J. Glimcher, *Rev. Mineral. Geochem.* **2006**, *64*, 223.
[20] T. Matsumoto, M. Okazaki, M. Inoue, Y. Hamada, M. Taira, J. Takahashi, *Biomaterials* **2002**, *23*, 2241.
[21] S. Koutsopoulos, E. Dalas, *Langmuir* **2001**, *17*, 1074.
[22] S. Koutsopoulos, E. Dalas, *J. Colloid Interface Sci.* **2000**, *231*, 207.
[23] S. Koutsopoulos, E. Dalas, *Langmuir* **2000**, *16*, 6739.
[24] T. Matsumoto, M. Okazaki, M. Inoue, J. Sasaki, Y. Hamada, J. Takahashi, *Dent. Mater. J.* **2006**, *25*, 360.
[25] G. M. Torrie, J. P. Valleau, *J. Comput. Phys.* **1977**, *23*, 187.
[26] S. Kumar, J. M. Rosenberg, D. Bouzida, R. H. Swendsen, P. A. Kollman, *J. Comput. Chem.* **1992**, *13*, 1011.
[27] D. A. McQuarrie, J. D. Simon, Molecular Thermodynamics, University Science Books, Sausalito, California. **1999**, 301.
[28] Z. J. Xu, X. N. Yang, Z. Yang, *J. Phys. Chem. B* **2008**, *112*, 13802.
[29] Y. Sun, B. N. Dominy, R. A. Latour, *J. Comput. Chem.* **2007**, *28*, 1883.
[30] B. Isralewitz, M. Gao, K. Schulten, *Curr. Opin. Struct. Biol.* **2001**, *11*, 224.
[31] C. Park, P. Fenter, Z. Zhang, L. Cheng, N. C. Sturchio, *Am. Mineral.* **2004**, *89*, 1647.
[32] A. Pareek, X. Torrelles, J. Rius, U. Magdans, H. Gies, *Phys. Rev. B* **2007**, *75*, 035418.
[33] A. Laio, M. Parrinello, *Proc. Natl. Acad. Sci.* **2002**, *99*, 12562.
[34] A. Laio, F. L. Gervasio, *Rep. Prog. Phys.* **2008**, *71*, 126601.
[35] J. Schneider, L. C. Ciacchi, *J. Am. Chem. Soc.* **2012**, *134*, 2407.
[36] N. Almora-Barrios, K. F. Austen, N. H. de Leeuw, *Langmuir* **2009**, *25*, 5018.
[37] S. Hauptmann, H. Dufner, J. Brickmann, S. M. Kast, R. S. Berry, *Phys. Chem. Chem. Phys.* **2003**, *5*, 635.
[38] B. R. Brooks, C. L. Brooks, A. D. Mackerell, L. Nilsson, R. J. Petrella, B. Roux, Y. Won, G. Archontis, C. Bartels, S. Boresch, A. Caflisch, L. Caves, Q. Cui, A. R. Dinner, M. Feig, S. Fischer, J. Gao, M. Hodoscek, W. Im, K. Kuczera, T. Lazaridis, J. Ma, V. Ovchinnikov, E. Paci, R. W. Pastor, C. B. Post, J. Z. Pu, M. Schaefer, B. Tidor, R. M. Venable, H. L. Woodcock, X. Wu, W. Yang, D. M. York, M. Karplus, *J. Comput. Chem.* **2009**, *30*, 1545.
[39] B. Hess, C. Kutzner, D. v. d. Spoel, E. Lindahl, *J. Chem. Theory Comput.* **2008**, *4*, 435.
[40] P. W. Tasker, *J. Phys. C: Solid State Phys.* **1979**, *12*, 4977.
[41] C. Rey, J. L. Miquel, L. Facchini, A. P. Legrand, M. J. Glimcher, *Bone* **1995**, *16*, 583.
[42] Y. Wu, J. L. Ackerman, H. M. Kim, C. Rey, A. Barroug, M. J. Glimcher, *J. Bone Miner. Res.* **2002**, *17*, 472.
[43] D. Zahn, O. Hochrein, *Phys. Chem. Chem. Phys.* **2003**, *5*, 4004.
[44] K. Makrodimitris, D. L. Masica, E. T. Kim, J. J. Gray, *J. Am. Chem. Soc.* **2007**, *129*, 13713.
[45] O. Hochrein, R. Kniep, D. Zahn, *Chem. Mater.* **2005**, *17*, 1978.
[46] W. L. Jorgensen, J. Chandrasekhar, J. D. Madura, R. W. Impey, M. L. Klein, *J. Chem. Phys.* **1983**, *79*, 926.
[47] M. Parrinello, A. Rahman, *J. Appl. Phys.* **1981**, *52*, 7182.
[48] S. Nosé, *J. Chem. Phys.* **1984**, *81*, 511.
[49] W. G. Hoover, *Phys. Rev. A* **1985**, *31*, 1695.
[50] T. Darden, D. York, L. Pedersen, *J. Chem. Phys.* **1993**, *98*, 10089.
[51] D. Taylor, *Br. Ceram. Trans. J.* **1988**, *87*, 88.
[52] F. J. A. L. Cruz, J. N. C. Lopes, J. C. G. Calado, M. E. M. d. Piedade, *J. Phys. Chem. B* **2005**, *109*, 24473.
[53] J. M. Soler, E. Artacho, J. D. Gale, A. García, J. Junquera, P. Ordejón, D. Sánchez-Portal, *J. Phys. Condens. Matter* **2002**, *14*, 2745.
[54] D. Sánchez-Portal, P. Ordejón, E. Artacho, J. M. Soler, *Int. J. Quantum Chem.* **1997**, *65*, 453.
[55] J. Junquera, Ó. Paz, D. Sánchez-Portal, E. Artacho, *Phys. Rev. B* **2001**, *64*, 235111.
[56] N. Troullier, J. L. Martins, *Phys. Rev. B* **1991**, *43*, 1993.
[57] J. P. Perdew, K. Burke, M. Ernzerhof, *Phys. Rev. Lett.* **1996**, *77*, 3865.
[58] H. F. Wang, Z.-P. Liu, *J. Phys. Chem. C* **2009**, *113*, 17502.
[59] Y. H. Fang, Z.-P. Liu, *J. Am. Chem. Soc.* **2010**, *132*, 18214.
[60] Y.-H. Fang, G.-F. Wei, Z.-P. Liu, *Catal. Today* **2013**, *202*, 98.
[61] I. Borukhov, D. Andelman, H. Orland, *Phys. Rev. Lett.* **1997**, *79*, 435.
[62] Y. F. Li, Z.-P. Liu, L. L. Liu, W. G. Gao, *J. Am. Chem. Soc.* **2010**, *132*, 13008.
[63] G.-F. Wei, Y.-H. Fang, Z.-P. Liu, *J. Phys. Chem. C* **2012**, *116*, 12696.
[64] W. L. Jorgensen, D. S. Maxwell, J. Tirado-Rives, *J. Am. Chem. Soc.* **1996**, *118*, 11225.
[65] H. J. C. Berendsen, J. R. Grigera, T. P. Straatsma, *J. Phys. Chem.* **1987**, *91*, 6269.
[66] S. Kerisit, S. C. Parker, *Chem. Commun.* **2004**, 52.
[67] S. Kerisit, S. C. Parker, *J. Am. Chem. Soc.* **2004**, *126*, 10152.
[68] U. Magdans, X. Torrelles, K. Angermund, H. Gies, J. Rius, *Langmuir* **2007**, *23*, 4999.
[69] S. Piana, F. Jones, J. D. Gale, *CrystEngComm* **2007**, *9*, 1187.
[70] S. Piana, F. Jones, J. D. Gale, *J. Am. Chem. Soc.* **2006**, *128*, 13568.
[71] A. Yin, H. C. Margolis, J. Grogan, Y. Yao, R. F. Troxler, F. G. Oppenheim, *Arch. Oral Biol.* **2003**, *48*, 361.
[72] S. Park, F. Khalili-Araghi, E. Tajkhorshid, K. Schulten, *J. Chem. Phys.* **2003**, *119*, 3559.
[73] I. Streeter, N. H. de Leeuw, *Proc. R. Soc. A* **2011**, *467*, 2084.
[74] T. Mori, R. J. Hamers, J. A. Pedersen, Q. Cui, *J. Chem. Theo. Comp.* in press.

Received: 14 June 2013
Revised: 1 September 2013
Accepted: 6 October 2013
Published online on 28 October 2013